ARTICLE

ACS chemical biology

A Ca^{2+}-Sensing Molecular Switch Based on Alternate Frame Protein Folding

Margaret M. Stratton, Diana M. Mitrea, and Stewart N. Loh*

Department of Biochemistry & Molecular Biology, State University of New York Upstate Medical University, 750 East Adams Street, Syracuse New York 13210

ABSTRACT Existing strategies for creating biosensors mainly rely on large conformational changes to transduce a binding event to an output signal. Most molecules, however, do not exhibit large-scale structural changes upon substrate binding. Here, we present a general approach (alternate frame folding, or AFF) for engineering allosteric control into ligand binding proteins. AFF can in principle be applied to any protein to establish a binding-induced conformational change, even if none exists in the natural molecule. The AFF design duplicates a portion of the amino acid sequence, creating an additional "frame" of folding. One frame corresponds to the wild-type sequence, and folding produces the normal structure. Folding in the second frame yields a circularly permuted protein. Because the two native structures compete for a shared sequence, they fold in a mutually exclusive fashion. Binding energy is used to drive the conformational change from one fold to the other. We demonstrate the approach by converting the protein calbindin D_{9k} into a molecular switch that senses Ca^{2+}. The structures of Ca^{2+}-free and Ca^{2+}-bound calbindin are nearly identical. Nevertheless, the AFF mechanism engineers a robust conformational change that we detect using two covalently attached fluorescent groups. Biological fluorophores can also be employed to create a genetically encoded sensor. AFF should be broadly applicable to create sensors for a variety of small molecules.

Molecules that produce a specific output signal in response to binding a target substrate offer the potential for developing novel biosensors, therapeutic agents, and diagnostic tools. Proteins are particularly effective in these roles because they can bind ligands with high affinity and specificity and are amenable to both *in vitro* and *in vivo* applications. The approach most often used to create protein-based sensors is to introduce fluorescence probes that report on binding-induced structural changes. A classic example is the calmodulin variant (cameleon) developed by Tsien and co-workers (*1, 2*). Cameleon is comprised of calmodulin with N- and C-terminal fusions of two green fluorescent protein (GFP) variants. Upon Ca^{2+} binding, calmodulin undergoes a dramatic conformational change that shortens the distance between GFPs and produces a fluorescence resonance energy transfer (FRET) output. Similarly, Hellinga, Dattelbaum, and colleagues have exploited the large conformational change of several bacterial periplasmic binding proteins (PBPs) to create various biosensors (*3–5*). PBPs bind their substrates in a flexible hinge region between two large domains. Fluorophores were attached to the protein to detect the interdomain closure that accompanies binding. Unlike calmodulin and PBPs, however, most proteins do not exhibit large-scale structural changes upon substrate binding.

How then can one develop a general mechanism for linking binding to an output signal? Toward this goal, Kohn and Plaxco progressively deleted amino acids from the C-terminus of an SH3 domain until it became so unstable that it unfolded (*6*). Binding to a target peptide induces refolding, which was detected by fluorescence of intrinsic Trp residues or of an extrinsic fluorophore. The success of this approach depends on the

*Corresponding author, lohs@upstate.edu.

Received for review July 25, 2008 and accepted September 28, 2008.

Published online October 24, 2008

10.1021/cb800177f CCC: $40.75

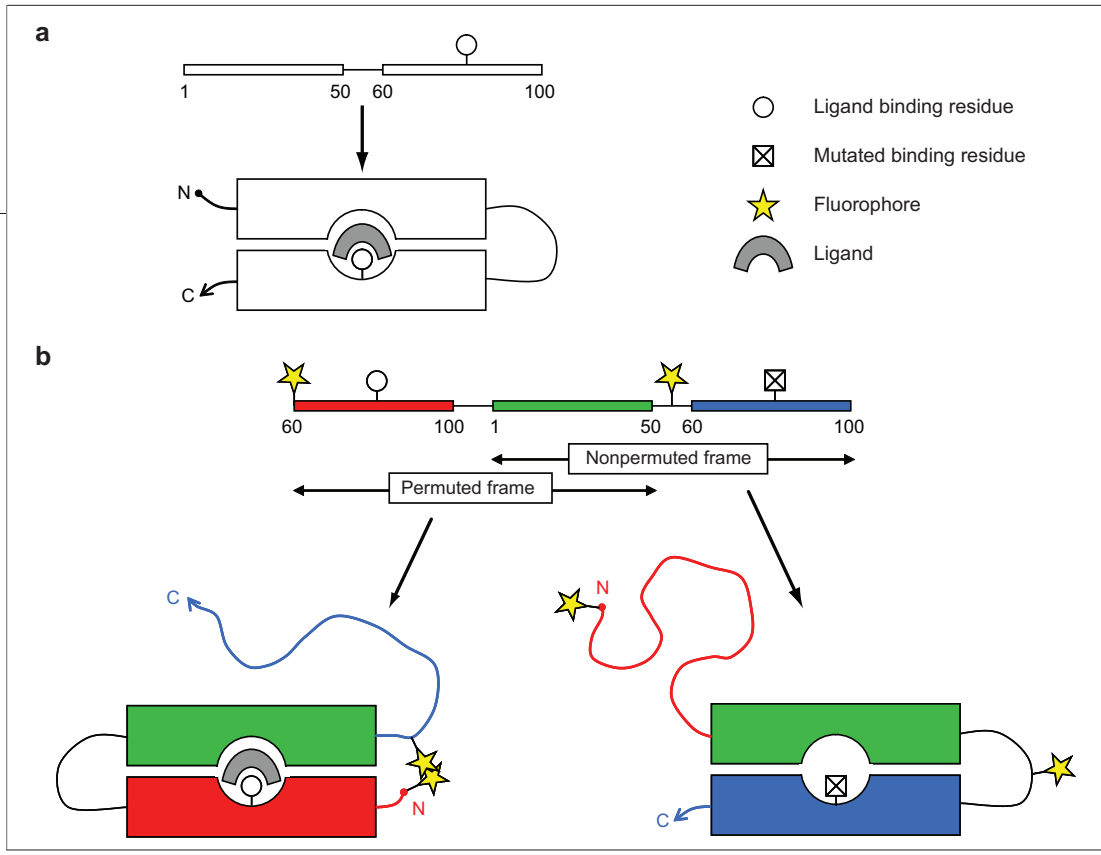

Figure 1. Schematic of the AFF mechanism for a hypothetical 100-amino-acid protein. a) Amino acid sequence (top) and structure (bottom) of the WT protein. A surface loop between residues 50 and 60 is depicted as a line. b) Amino acid sequence (top) and structures (bottom) of the AFF variant. Amino acids are numbered according to the WT sequence. The duplication consists of residues 60−100 (red) plus a short peptide used to link the original N- and C-termini in the permuted structure (shown as a line between residues 100 and 1). The region shared between permuted and nonpermuted folds is depicted in green, and the original residues 60−100 are colored blue. The protein can fold in the permuted frame (left) or the nonpermuted frame (right) but not in both. Ligand binding drives the equilibrium between the two conformations to the permuted fold. Fluorophores are placed at the N-terminus and in the surface loop between residues 50 and 60.

protein unfolding upon truncation, remaining soluble and intact in the unfolded state, and being able to refold upon ligand binding. In addition, suitable locations for fluorophore placement must be determined on a case-by-case basis, with no assurance that binding can be made to produce an optical change of requisite intensity.

Here, we introduce the concept of alternate frame folding (AFF) as a means to couple ligand binding to protein conformational change in a simple, predictable, and well-defined manner. Like the approach taken by Kohn and Plaxco, our strategy exploits a folding reaction. However, the protein is native in both ligand-bound and ligand-free states. What is new is the mechanism by which binding-induced folding is coupled to unfolding of a distant region of the molecule. The protein structure is *remodeled* upon binding; no net folding or unfolding occurs.

The AFF design entails two modifications to the amino acid sequence. To illustrate, consider a hypothetical 100-amino-acid protein whose substrate binding pocket is formed by both N- and C-terminal portions of the molecule (Figure 1, panel a). The amino acid sequence is shown at top, and a schematic of the three-dimensional structure is depicted at bottom. Residues 50−60 form a surface loop. The C-terminal portion of the molecule (amino acids 60−100), which contains at least one ligand binding residue, is duplicated and fused to the N-terminus of the protein using a short peptide linker (Figure 1, panel b). This step resembles an earlier study in which a bifunctional protein was created by the partial overlap of two unrelated protein sequences (*7*) and another study where an α-helix was duplicated in T4 lysozyme to introduce a guanidinium ion binding site (*8*). In our design, the resulting fusion protein can fold in one of two frames. The first corresponds to the wild-type (WT) sequence, and folding produces the normal structure. Folding in the other frame produces a circularly permuted protein. The original N- and C-termini are joined by the short peptide linker, and the new termini are located at the solvent-exposed loop. The two folds compete for the shared sequence (shown in green). Consequently, the protein folds in a mutually exclusive fashion. It can fold in the nonpermuted frame or the permuted frame but not both. The two native forms are populated according to their thermodynamic stabilities. This balance can be adjusted by introducing stabilizing or destabilizing mutations into one of the frames.

The second modification is the mutation of one or more ligand binding amino acids in one of the duplicated segments. The mutation is shown in the nonpermuted frame in Figure 1, panel b, since the nonper-

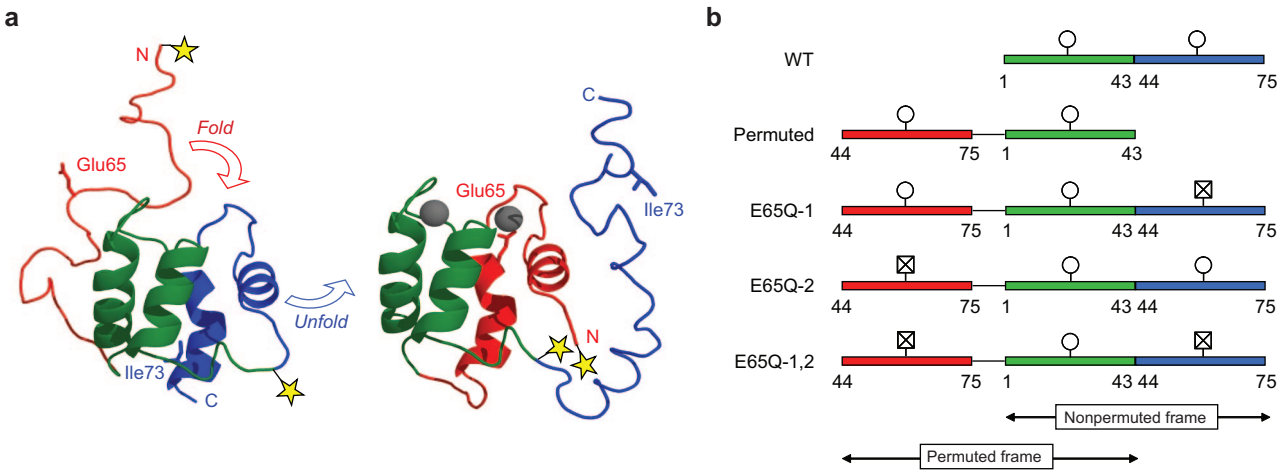

Figure 2. Design of calbindin-AFF. a) Predicted structures of calbindin-AFF E65Q-1 in nonpermuted (left) and permuted (right) conformations. Color coding is the same as in Figure 1. The duplicate EF-hands are depicted as unfolded N-terminal and C-terminal tails in the nonpermuted and permuted structures, respectively. Glu65 is indicated in the permuted frame (red segment). Ca^{2+} (gray sphere) drives remodeling of the structure so that the side chain of Glu65 is presented for binding. Ile73 (mutated to Cys73 for thiol exchange experiments) is indicated in the nonpermuted frame (blue segment). Ca^{2+} binding causes the blue segment to unfold, exposing the side chain of residue 73 to the solvent. This conformational change exchanges the positions of the termini and the loop connecting the EF-hands, causing the fluorophores to change proximity. b) Amino acid sequences of calbindin variants created in this study. Amino acids are numbered according to the WT sequence. Symbols are the same as in Figure 1. A 6-amino-acid linker is used to join the original N- and C-termini in the permuted structure; this peptide is shown as a line between residue 75 and residue 1.

muted fold is generally expected to be more stable than the permuted fold. Upon addition of ligand, the natural coupling between binding and folding drives a conformational change to the permuted fold. The binding site is now remodeled so that the critical binding residue can make contact with the substrate. AFF establishes a mechanism by which folding of one portion of the molecule is coupled to unfolding of another. Folding in the nonpermuted and permuted frames is expected to produce proteins with disordered N- or C-terminal tails, respectively, which are composed of the duplicated polypeptide. The unstructured segment folds and exchanges with its counterpart to form a functional binding pocket. The formerly structured segment becomes a disordered tail. The conformational shift is from one native structure to another, but a significant topological change has occurred. By placing fluorescent groups at two sites that change proximity between conformations, this shift is harnessed to an optical output (Figure 1, panel b).

AFF offers the following advantages over existing protein switches: (i) The target protein does not need to exhibit a pre-existing conformational change. (ii) Only a segment of the protein is unstructured in either conformation. Since this segment can be small and exists as a tail extending from one of the termini, the potential for misfolding and/or aggregation is minimized. (iii) The placement of fluorophores follows naturally from the AFF design. The two positions that experience the greatest distance change upon binding-induced remodeling are at one of the termini and at a solvent-exposed loop of choice (Figure 1, panel b). Introduction of fluorophores at these sites is expected to be relatively nonperturbing. (iv) Our design is compatible with biological fluorophores (*e.g.*, GFP variants) for *in vivo* applications. (v) AFF can in principle be applied to any ligand-binding protein, with the exception of those containing disulfide cross-links between the shared and duplicated segments of the molecule.

RESULTS AND DISCUSSION

Structural and Thermodynamic Characterization of Calbindin Variants. We tested the AFF mechanism using the 75-amino-acid protein calbindin D_{9k}. Calbindin binds two Ca^{2+} ions *via* a pair of EF-hands that are connected by a loop centered around residue 43. The X-ray

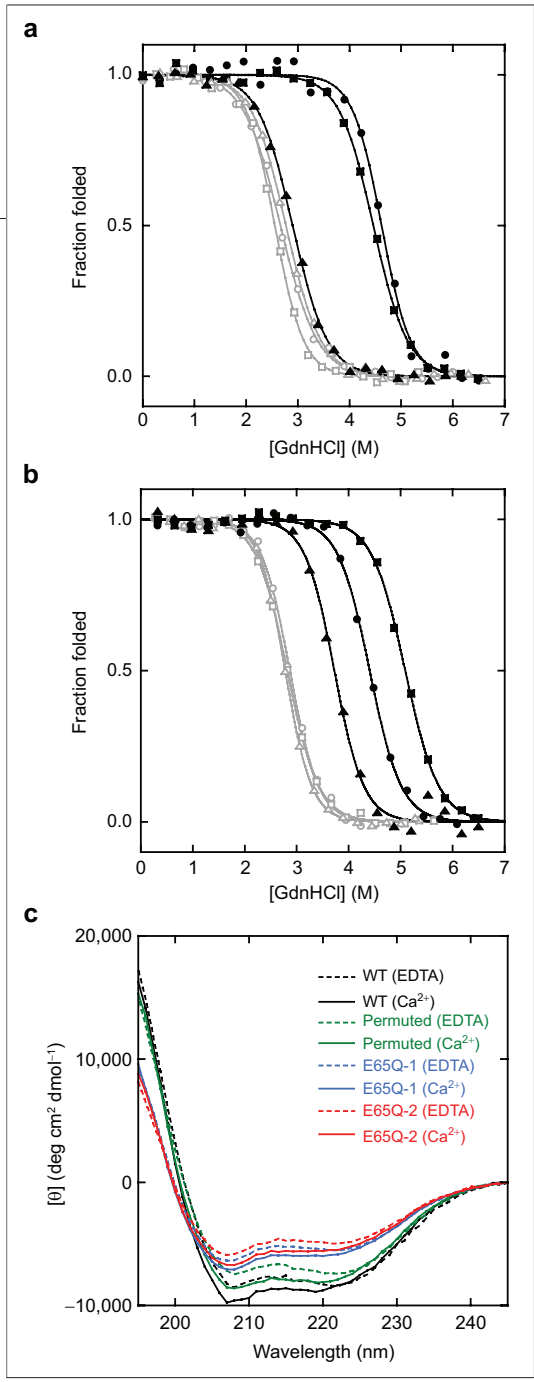

Figure 3. Structural and thermodynamic characterization of calbindin variants. a) GdnHCl-induced unfolding of WT calbindin (squares), permuted calbindin (circles), and E65Q calbindin (triangles), monitored by CD ellipticity at 222 nm. Open symbols/gray lines and closed symbols/black lines represent data collected in the presence of 100 μM EDTA and 100 μM $CaCl_2$, respectively. Lines are best fits of the data to the linear extrapolation equation $\Delta G = \Delta G^{H_2O} - m$[GdnHCl], where ΔG^{H_2O} is the folding free energy in the absence of denaturant and m is the cooperativity parameter. b) GdnHCl-induced unfolding of calbindin-AFF E65Q-1 (circles), calbindin-AFF E65Q-2 (squares), and calbindin-AFF E65Q-1,2 (triangles). Open symbols/gray lines and closed symbols/black lines represent data collected in the presence of 100 μM EDTA and 100 μM $CaCl_2$, respectively. c) CD wavelength scans of calbindin variants. Samples contain 100 μM EDTA or 100 μM $CaCl_2$ as indicated.

crystal structure of WT calbindin (*9*) is shown in green and blue in Figure 2, panel a (left structure). Protein−protein interactions between the EF-hands cause Ca^{2+} to bind cooperatively with dissociation constants (K_d) of ~1 and ~0.1 μM (*10*). We first determined the effect of permutation on stability and function. Calbindin was permuted at position 43, and the original termini were joined by a 6-amino-acid linker. The permutant is predicted to adopt the conformation shown in green and red in Figure 2, panel a (right structure), in which the original surface loop and termini have exchanged positions. The amino acid sequences of all calbindin variants are summarized in Figure 2, panel b. Guanidine hydrochloride (GdnHCl) denaturation curves (Figure 3, panel a) reveal that the folding free energy (ΔG^{H_2O}) of permuted calbindin is slightly higher than that of WT in their Ca^{2+}-free (apo) states (Table 1). This finding is surprising, since permutation typically destabilizes proteins. The N- and C-termini of calbindin are close, and the loop connecting the EF-hands is flexible (*11*). These factors may account for the high stability of the permutant. Figure 3, panel a suggests that the permuted and nonpermuted folds will be populated to comparable extents in the absence of Ca^{2+}.

Permuted calbindin binds Ca^{2+}, as evidenced by the shift in unfolding transition to higher [GdnHCl] (Figure 3, panel a) and by altered mobility in native polyacrylamide gel shift assays (Figure 4). Circular dichroism (CD) spectra (Figure 3, panel c) indicate that the secondary structures of WT and permuted calbindin are similar. The Glu65 side chain ligates Ca^{2+} (Figure 2, panel a), and the E65Q mutation reduces affinity by 10^5-fold (*12*). The stability of apo-E65Q calbindin is close to that of apo-WT (Table 1), suggesting that the E65Q substitution will not significantly perturb the equilibrium between permuted and nonpermuted folds. Addition of 100 μM Ca^{2+} stabilizes E65Q by only 0.4 kcal mol^{-1} compared to 4.2 kcal mol^{-1} for WT. This finding is consistent with Ca^{2+} binding to only the N-terminal EF-hand in the E65Q variant.

Calbindin-AFF was constructed by duplicating the C-terminal EF-hand (residues 44−75) and fusing it to the N-terminus of calbindin (Figure 2). A 6-amino-acid linker was introduced to bridge the original N- and C-termini. The C-terminal hand is largely disordered in isolation and folds upon binding to Ca^{2+} (*13*). Three constructs were made in which the E65Q mutation was placed into the nonpermuted frame of calbindin-AFF (E65Q-1), the permuted frame (E65Q-2), or both frames (E65Q-1,2) (Figure 2, panel b). Mass spectrometry (not shown) reveals that all AFF constructs express as soluble, full-length proteins in *E. coli*. Figure 3, panel b and Table 1 show that they are folded and stable in their apo forms, with ΔG^{H_2O} values comparable to those of WT and permuted calbindin. Figure 3, panel b and the native gel shift assays of Figure 4 confirm that calbindin-AFF binds Ca^{2+}. Ca^{2+} binding stabilizes calbindin-AFF E65Q-1,2 to a greater extent than it does E65Q ($\Delta\Delta G^{H_2O}$ = 1.2 and 0.4 kcal mol^{-1}, respectively). The reason is not clear, although the magnitude of stabilization is notably less than that of the calbindin variants that possess two functional EF-hands.

The CD spectra of the AFF variants indicate that they contain significantly less helical structure than either

TABLE 1. Thermodynamic parameters for folding of calbindin variants[a]

	ΔG^{H_2O} (kcal mol^{-1})		m (kcal mol^{-1} M^{-1})		C_m (M)	
Variant	EDTA	Ca^{2+}	EDTA	Ca^{2+}	EDTA	Ca^{2+}
WT	3.92	8.29	1.53	1.82	2.56	4.55
permuted	5.54	7.98	1.99	1.78	2.78	4.49
E65Q	4.28	4.68	1.53	1.64	2.80	2.85
E65Q-1	4.78	8.04	1.71	1.58	2.80	5.09
E65Q-2	4.91	7.70	1.76	1.74	2.79	4.42
E65Q-1,2	5.65	6.84	2.05	1.84	2.76	3.72

[a]Standard deviations are ±0.4 kcal mol^{-1} (ΔG^{H_2O}) and ±0.1 kcal mol^{-1} M^{-1} (m). C_m is the midpoint of GdnHCl-induced unfolding.

WT or permuted calbindin (Figure 3, panel c). WT apo-calbindin exhibits a $[\theta]_{222}$ value of −8,500 deg cm^2 dmol^{-1}, which corresponds to a helix content of 20% (*14*). This percentage is lower than that expected from the crystal structure (57%). The discrepancy is likely due to uncertainty in protein concentration associated with the low extinction coefficient of calbindin (1280 M^{-1} cm^{-1} at 280 nm (*15*)). Calbindin contains no Trp residues and only a single Tyr, making concentration determination particularly susceptible to the presence of protein contaminants. To address this problem, we normalized the calbindin concentrations by running CD samples on SDS−PAGE and integrating densities of the stained bands (see Methods). Thus, although the absolute protein concentration is uncertain, the relative concentrations are known more accurately and CD spectra of variants can be compared directly. The AFF constructs E65Q-1 and E65Q-2 display $[\theta]_{222}$ values of −5,500 and −5,000 deg cm^2 dmol^{-1}, respectively, corresponding to a 35−41% decrease in helix content relative to WT. These data agree with the previous report that the isolated C-terminal EF-hand is unfolded in the absence of Ca^{2+} (*13*) and suggest that the duplicated C-terminal hand in calbindin-AFF is similarly unstructured. Figure 3, panel b also demonstrates that Ca^{2+} binding does not change the helix content of any of the AFF variants. No net folding occurs upon binding.

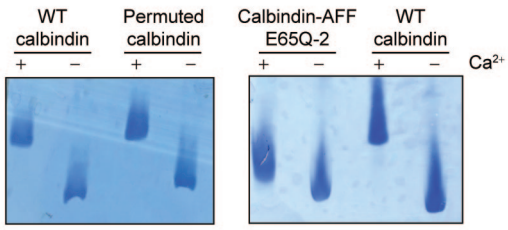

Figure 4. Native polyacrylamide gel shift assays in the presence (+) and absence (−) of 2 mM $CaCl_2$. Samples that lack $CaCl_2$ contain 2 mM EDTA.

Fluorescence Tests of the AFF Mechanism. One of the benefits of AFF is that fluorophore placement follows naturally from the design. Two specific positions in the amino acid sequence are expected to be spatially distant from each other in one fold and close in the second fold. These positions correspond to the N-terminus of the protein and the site of permutation (a surface loop in the nonpermuted frame). These locations are inherently nonperturbing with respect to fluorophore placement. To illustrate, we attached one pyrene group to the N-terminus of calbindin-AFF and another to amino acid 43 of the nonpermuted frame (Figure 2). Pyrene groups were introduced by first inserting Cys residues proximal to the described locations and labeling using maleimide chemistry. In the nonpermuted fold, the pyrene groups are separated by a stretch of unstructured polypeptide and hence are distant from one another (Figure 2, panel a). In the permuted fold, the two Cys residues adopt the equivalent of consecutive positions in the surface loop that connects the EF-hands in the WT structure. Close proximity of the pyrene groups is reported by the appearance of a fluorescence excimer band at 475 nm (*16*). Alternately, one can label the protein at the C-terminus and at amino acid 43 of the permuted frame. This pairing reverses the distance change upon binding and inverts the output signal.

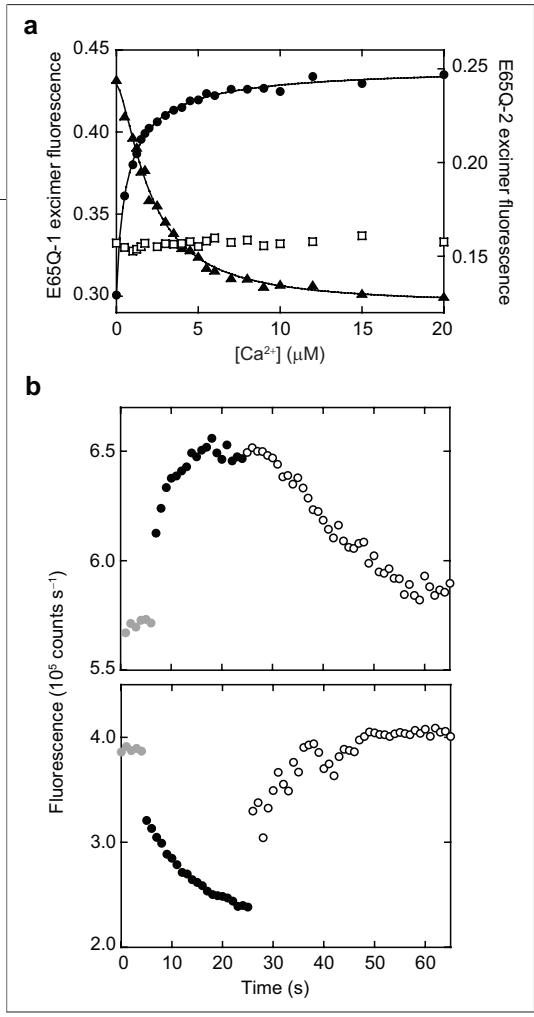

Figure 5. Fluorescence tests of the switching mechanism. a) Ca^{2+} binding to calbindin-AFF E65Q-1 (circles), E65Q-2 (triangles), and E65Q-1,2 (squares), monitored by the ratio of excimer fluorescence (475 nm) to monomer fluorescence (383 nm). Lines are best fits of the data to the Hill equation ($Y = A + B[Ca^{2+}]^n/([Ca^{2+}]^n + (K_d)^n)$), where *A* is initial fluorescence, *B* is the amplitude, and *n* is the Hill coefficient. Data for E65Q-1,2 are plotted on the same *y*-axis as the data for E65Q-2. b) Kinetics of conformational changes associated with Ca^{2+} binding (black circles) and Ca^{2+} release (open circles), monitored by excimer fluorescence at 475 nm. E65Q-1 and E65Q-2 are shown in the upper and lower panels, respectively. Gray circles are initial fluorescence values of the apo-proteins. $CaCl_2$ (20 μM) and EDTA (50 μM) were added at the times indicated ($t \approx 5$ s and $t \approx 25$ s, respectively).

We tested the switching mechanism using E65Q-1. Addition of Ca^{2+} increases excimer fluorescence, consistent with the expected nonpermuted to permuted fold shift (Figure 5, panel a). An alternate explanation is that the unstructured EF-hand binds Ca^{2+} and folds. This event could potentially produce a fluorescence change without a fold shift. However, as predicted by the models in Figure 1 and Figure 2, CD spectra detect no change in secondary structure upon titration of Ca^{2+} (Figure 3, panel c). A critical test of the AFF mechanism is whether the switch can be inverted by changing the placement of the binding mutation. To this end, we moved the E65Q mutation to the permuted frame. Ca^{2+} binding results in a fluorescence decrease in E65Q-2, indicating that the switch has reversed directions from the permuted to the nonpermuted fold (Figure 5, panel a). We were able to detect both fold shifts because permuted and nonpermuted folds are populated in the absence of Ca^{2+} (Figure 3, panel a). Fitting the data to the Hill binding equation yields $K_d = 0.69 \pm 0.3$ μM, $n = 0.90 \pm 0.1$ (E65Q-1) and $K_d = 2.1 \pm 0.2$ μM, $n = 1.5 \pm 0.1$ (E65Q-2). Finally, no change in excimer fluorescence is observed for E65Q-1,2 (Figure 5, panel a) as neither fold is favored by Ca^{2+} binding.

Rates of conformational change were measured by monitoring pyrene excimer fluorescence over time. Adding EDTA to the Ca^{2+}-bound proteins causes fluorescence values to return to those of the unbound states (Figure 5, panel b). Conformational rearrangements associated with Ca^{2+} binding and release are complete within ~30 s. As in Figure 5, panel a, E65Q-1 and E65Q-2 produce fluorescence changes of opposite sign. The switching mechanism is thus rapid and fully reversible.

Structural Test by Thiol-Disulfide Exchange. As an independent test of the mechanism, we monitored Ca^{2+}-driven folding/unfolding of the duplicated EF-hand. The I73C mutation was introduced into the C-terminal EF-hand (blue segment of Figure 2) of otherwise Cys-free E65Q-1. To preserve the thermodynamic balance between the 2-folds, we introduced the compensatory I73S mutation into the duplicate EF-hand of the permuted frame (red segment of Figure 2). CD wavelength scans and denaturation experiments (not shown) reveal that the I73C/I73S variant is folded and stable ($\Delta G^{H_2O} = 4.4$ kcal mol^{-1}) and that stability increases in the presence of 100 μM Ca^{2+} ($\Delta\Delta G^{H_2O} = 1.8$ kcal mol^{-1}). The Ile73 side chain is buried in the interface between EF-hands (Figure 2, panel a). If calbindin-AFF adopts the nonpermuted fold, Cys73 is predicted to be buried and protected from thiol-reactive reagents. Upon addition of Ca^{2+}, the protein is predicted to shift to the permuted fold, causing the C-terminal EF-hand (blue in Figure 2, panel a) to unfold and expose Cys73. Exposure of the Cys73 thiol group is monitored by its reactivity with dithiobis(2-nitrobenzoic acid) (DTNB) (*17*).

In the absence of Ca^{2+}, the increase in TNB absorbance is minimally fit by two exponentials with rate constants $k_{fast} = 2.5$ s^{-1} (57% total amplitude) and $k_{slow} = 0.26$ s^{-1} (43% total amplitude) (Figure 6). The value of log *k* increases linearly with log [DTNB] (data not shown), indicating that exchange follows the EX2 mechanism. The free energy of the structural opening event (ΔG_{op}) that exposes the side chain to exchange can therefore be calculated using $\Delta G_{op} = RT \ln P$, where the protection factor *P* is the intrinsic exchange rate divided by the observed rate. To obtain the intrinsic rate, we monitored exchange of denatured I73C/I73S in the presence of 4.5−7.0 M GdnHCl. The observed rate varied linearly over that GdnHCl concentration range, yield-

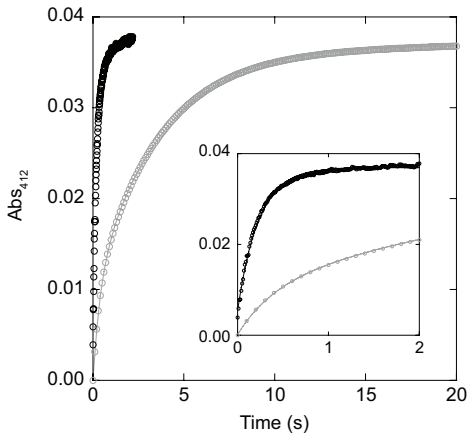

Figure 6. Structural test of the switching mechanism. Solvent accessibility of Cys73 in the I73C/I73S variant of calbindin-AFF E65Q-1, as determined by DTNB exchange rates. The appearance of the TNB leaving group is monitored by absorbance at 412 nm. Black and gray circles indicated the presence of 100 μM $CaCl_2$ and 100 μM EDTA, respectively. The inset shows time points between 0 and 2 s. The gray line is the best fit to a double-exponential function (k_{fast} = 2.5 s^{-1}, 57% total amplitude; k_{slow} = 0.26 s^{-1}, 43% total amplitude). The black line is the best fit to a single exponential function (k = 4.2 s^{-1}).

ing a slope of -0.22 s^{-1} M^{-1} and an extrapolated intrinsic rate of 2.0 s^{-1} in the absence of denaturant (data not shown).

The most straightforward interpretation of the biphasic absorbance increase is that there are two populations of exchanging species in slow equilibrium; 57% of the molecules exchange with $P = 0.8$, revealing that the environment around Cys73 is unstructured, while 43% of the molecules exhibit a P value of 7.7, indicating burial of Cys73 with $\Delta G_{op} = 1.2$ kcal mol^{-1}. The populations are consistent with those predicted from the stabilities of WT and permuted calbindin.

In the presence of Ca^{2+}, exchange becomes significantly faster and the data are fit by a single exponential with a rate constant of 4.2 s^{-1} ($P = 0.5$) (Figure 6). Cys73 is thus fully exposed in all molecules. Ca^{2+} binding stabilizes calbindin (Figure 3, panels a and b) and is known to decrease rates of amide hydrogen exchange (*18, 19*). Therefore, the overall increase in exchange rate that we observe is best explained by unfolding of the C-terminal EF-hand upon Ca^{2+}-induced fold switching. Moreover, that hand appears to be similarly unstructured in the fraction of molecules that adopt the permuted fold in the absence of Ca^{2+}. These findings are consistent with the decrease in helix content observed for the AFF variants (Figure 3, panel c).

General Considerations. We have shown that AFF can introduce a binding-induced conformational change into calbindin, a protein that possesses no allosteric behavior in its natural form. We now discuss the limitations, strengths, and potential of this technology. The main limitations are that the protein must tolerate permutation and partial sequence duplication without aggregating or otherwise losing function. Circular permutation occurs in nature and is one of the mechanisms for generating protein diversity during evolution (*20*). In the laboratory, numerous proteins encompassing different types of folds have been shown to retain structure, function and stability upon permutation, including GFP and related variants (*21, 22*), SH3 domains (*23*), PDZ domains (*24*), antibody variable chain (*25*), and others (*26–32*). It is reasonable to expect that many proteins, if not most, will be amenable to this modification, particularly since one can typically choose different permutation sites from multiple surface loops. In that regard, computational methods can assist in predicting viable permutation sites (*33*).

Perhaps of greater concern is whether the presence of an unfolded tail will lead to misfolding, aggregation, or degradation. Kohn and Plaxco (*6*) demonstrated that a fully unfolded protein can be an effective sensor *in vitro*. Unfolded proteins may be less viable for *in vivo* applications, however, as molecular crowding and endogenous proteases increase the risk of aggregation and degradation in the cell. AFF is advantageous because the protein is native in both the bound and unbound states. The length of the unfolded segment depends on the locations of binding residues. That sequence can be short provided that a binding residue is close to one of the termini. For example, consider the hypothetical 100-amino-acid protein in Figure 1, panel b. In principle, the permutation site can be at any surface loop or turn. If a critical binding residue is near the C-terminus (*e.g.*, position 90), the permutation site is chosen to be the closest loop to the left of position 90 (*e.g.*, position 80). The tail is only 20 amino acids long. If the binding residue is near the N-terminus (*e.g.*, position 10), then the permutation site is chosen to be the closest loop to the right of position 10 (*e.g.*, position 20). Amino acids 1−20 are then duplicated and

appended to the C-terminus of the protein. The length of the duplicated segment is again 20 amino acids. Thus, the tail is never more than 50% of the WT sequence and can be considerably less. Calbindin can be permuted at only one location; it has three surface loops and two are used to bind Ca^{2+}. Larger proteins, however, will generally contain many loops that can serve as candidate permutation sites.

Transferring the E65Q mutation from one frame to the other reverses the calbindin-AFF switch and inverts the output signal. While this finding constitutes an important test of the AFF mechanism, it also suggests that sensitivity can be optimized. The permuted and nonpermuted folds appear to be populated to approximately equal extents. When the equilibrium constant between folds is unity, the fluorescence signal can change by at most 2-fold. The solution is to introduce a "tuning" mutation into one of the duplicated segments. Tuning mutations either stabilize or destabilize the protein when it is folded in that particular frame. For example, the F66W substitution modestly decreases calbindin stability ($\Delta\Delta G^{H_2O} = -2.3$ kcal mol^{-1}) (*34*) and has little effect on Ca^{2+} binding affinity (*10*). If it were placed in the permuted frame of E65Q-1, fluorescence output can theoretically increase by up to exp(2.3/*RT*), or 50-fold, on Ca^{2+} binding. The increase in signal change comes at the expense of binding affinity, as a portion of binding energy is used to drive the unfavorable conformational change. Optimal sensitivity can be attained by choosing tuning mutations that balance signal change with binding affinity.

The technology developed here establishes a pathway for creating custom sensors that bind biologically relevant ligands as well as environmentally significant molecules. Rational design and directed evolution approaches have already demonstrated that proteins can be made to bind scores of target molecules. AFF is a straightforward modification that can potentially be applied to many of these proteins. Biological fluorophores such as GFP FRET pairs can be employed in place of pyrene or other extrinsic groups to generate fully genetically encoded sensors. For that application, the protein must tolerate insertion of GFP into one of its surface loops. This condition can be met in favorable cases, provided that the proteins are joined by linker peptides of sufficient length (*35*).

METHODS

Gene Construction. The plasmid bearing the bovine calbindin D_{9k} gene (P43M variant; designated WT throughout the text) was a gift from W. Chazin (Vanderbilt University). The calbindin-AFF gene was constructed by polymerase chain reaction of the coding sequence for amino acids 44−75, with primers introducing NdeI and NotI restriction sites. A nucleotide sequence corresponding to a 6-amino-acid linker (GGAAAM) was placed at the 3′ end. This construct was subsequently ligated to the 5′ end of the calbindin gene. Mutations (E65Q, I73C, I73S) and insertions (Cys) were introduced at the sites described in the text using the QuikChange mutagenesis kit (Stratagene). All genes were fully sequenced.

Protein Expression and Purification. Calbindin-AFF plasmids were transformed into *E. coli* BL21(DE3) cells. Cells were grown at 37 °C and induced with 0.1 g L^{-1} IPTG at $OD_{600} = 0.6$. WT and permuted calbindin were expressed for 3−6 h at 37 °C. Calbindin-AFF variants were expressed for 10−12 h at 20 °C. Cell pellets were resuspended in 20 mM imidazole (pH 6), 0.1 mM EDTA, 5 mM β-mercaptoethanol, and lysed by a small amount of lysozyme. The lysate was sonicated and centrifuged, and the pellets were discarded. Solution pH was lowered to 4.3 by addition of 1/10 volume 0.8 M sodium acetate (pH 4.3). After centrifugation, the supernatant contained approximately 80% pure calbindin-AFF. The pH was raised to ~7 with 1 M Tris base, and the solution was dialyzed against 20 mM imidazole (pH 6), 0.1 mM EDTA, 5 mM β-mercaptoethanol. The solution was then loaded onto a Fast-Flow DEAE column (Bio-Rad) and eluted with a 0−1.0 M NaCl gradient. The purity of the final product was ≥95% as judged by SDS−PAGE. The molecular weight of calbindin-AFF was determined to be 12,992 Da by mass spectrometry (expected MW = 12,986 Da).

GdnHCl Denaturation Experiments. Solutions used in all experiments were treated with Chelex 100 to remove trace metal ions. Protein samples were prepared by mixing a solution of protein (2−5 μM) in buffer (10 mM sodium phosphate (pH 7), 2 mM dithiothreitol, and either 100 μM $CaCl_2$ or 100 μM EDTA) with an identical solution containing 6.5 M GdnHCl. Dilutions were made using a Hamilton Microlab 540B dispenser and denaturant concentrations were measured by refractive index (*36*). Samples were equilibrated overnight at 10 °C. CD data were collected at 10 °C on an Aviv model 202 spectropolarimeter. Data were fit to the two-state linear extrapolation equation (*37*).

Circular Dichroism Experiments. Protein concentrations were initially calculated by diluting stock solutions (10 mM sodium phosphate, pH 7) into 7 M GdnHCl and measuring absorbance at 280 nm ($\varepsilon_{280} = 1280$ M^{-1} cm^{-1} (*15*)). CD samples were prepared by diluting identical volumes of each protein into 10 mM sodium phosphate (pH 7). Molar ellipticity values of permuted calbindin (the most pure of the variants) were calculated assuming 100% purity. To correct for any error in calbindin concentration introduced by the presence of protein contaminants, identical volumes of the stock solutions were run on a 12% polyacrylamide tris-tricine gel and stained with coomassie brilliant blue. Relative intensities of the calbdindin bands were measured in triplicate using the ImageJ program (http://rsweb.nih.gov/ij/). Band intensity ratios were calculated relative to that of permuted calbindin. Molar ellipticity values of the other variants were multiplied by those ratios to generate the spectra shown in Figure 3, panel b.

Pyrene Labeling. Protein samples were treated with 10 mM Tris(2-carboxyethyl) phosphine (TCEP) to fully reduce thiols, and 1 mM EDTA to remove any residual Ca^{2+}. TCEP and EDTA were removed by precipitating the protein twice using trichloroacetic acid. Pellets were dissolved in 10 mM sodium phosphate (pH 6.5), 7 M GdnHCl to a final protein concentration of 0.15 mM. *N*-1-Pyrene maleimide (Anaspec) was added to a final concentration of 0.5 mM, and the reaction was allowed to proceed for 2−5 h at 20 °C in the dark. The reaction was terminated, and the protein refolded by twice desalting the solution into 50 mM Tris (pH 7.5), 0.1 M NaCl using a PD-10 column (Amersham). Protein samples were stored at −20 °C and thawed immediately before use.

Ca^{2+} Binding Experiments. Pyrene labeled protein samples were diluted to 12 μM in 50 mM Tris (pH 7.5), 0.1 M NaCl. Ca^{2+} titrations were performed by adding small aliquots of ultrapure $CaCl_2$ solutions. Fluorescence data were collected at 20 °C on a Jobin-Yvon/SPEX Fluoromax-3 fluorimeter with excitation set to 345 nm. Excimer fluorescence was normalized to protein concentration by the ratio of the excimer peak (475 nm) to the monomer peak (383 nm).

Native polyacrylamide gel (12%) Ca^{2+} binding assays were performed as described previously (*38*).

Thiol-Disulfide Exchange Experiments. Proteins (~15 μM) were mixed with DTNB (150 μM) in 50 mM Tris (pH 7.5) using a Bio-Logic SM-4 stop-flow instrument. Liberation of the TNB group was monitored by absorbance at 412 nm. Intrinsic exchange rates were measured by the same procedure, except protein and DTNB solutions were equilibrated in 4.5−7.0 M GdnHCl for at least 2 h prior to measurements. All data were recorded at 20 °C.

Acknowledgment: We thank J.-H. Ha for discussions, L. Parsons and Q. Xu for technical assistance, and W. Chazin for the calbindin plasmid. This work was supported by NIH grant GM069755 to S.N.L. M.M.S. performed all experiments and cowrote the manuscript with S.N.L.; D.M.M. contributed to the conception of the AFF mechanism.

REFERENCES

1. Miyawaki, A., Llopis, J., Heim, R., McCaffery, J. M., Adams, J. A., Ikura, M., and Tsien, R. Y. (1997) Fluorescent indicators for Ca^{2+} based on green fluorescent proteins and calmodulin, *Nature 388*, 882–887.
2. Giepmans, B. N. G., Adams, S. R., Ellisman, M. H., and Tsien, R. Y. (2006) The fluorescent toolbox for assessing protein location and function, *Science 312*, 217–224.
3. Vercillo, N. C., Herald, K. J., Fox, J. M., Der, B. S., and Dattelbaum, J. D. (2007) Analysis of ligand binding to a ribose biosensor using site-directed mutagenesis and fluorescence spectroscopy, *Protein Sci. 16*, 362–368.
4. De Lorimer, R. M., Smith, J. J., Dwyer, M. A., Looger, L. L., Sali, K. M., Paavola, C. D., Rizk, S. S., Sadigov, S., Conrad, D. W., Loew, L., and Hellinga, H. W. (2002) Construction of a fluorescent biosensor family, *Protein Sci. 11*, 2655–2675.
5. Dwyer, M. A., and Hellinga, H. W. (2004) Periplasmic binding proteins: a versatile superfamily for protein engineering, *Curr. Opin. Struct. Biol. 14*, 495–504.
6. Kohn, J. E., and Plaxco, K. W. (2005) Engineering a signal transduction mechanism for protein-based biosensors, *Proc. Natl. Acad. Sci. U.S.A. 102*, 10841–10845.
7. Sallee, N. A., Yeh, B. J., and Lim, W. A. (2007) Engineering modular protein interaction switches by sequence overlap, *J. Am. Chem. Soc. 129*, 4606–4611.
8. Yousef, M. S., Baase, W. A., and Matthews, B. W. (2004) Use of sequence duplication to engineer a ligand-triggered, long distance molecular switch in T4 lysozyme, *Proc. Natl. Acad. Sci. U.S.A. 101*, 11583–11586.
9. Szebenyi, D. M., and Moffat, K. (1986) The refined structure of vitamin D-dependent calcium binding protein from bovine intestine. Molecular details, ion binding, and implications for the structure of other calcium-binding proteins, *J. Biol. Chem. 261*, 8761–8777.
10. Kragelund, B. B., Jonsson, M., Bifulco, G., Chazin, W. J., Nilsson, H., Finn, B. E., and Linse, S. (1998) Hydrophobic core substitutions in calbindin D_{9k}: effects on Ca^{2+} binding and dissociation, *Biochemistry 37*, 8926–8937.
11. Skelton, N. J., Kordel, J., and Chazin, W. J. (1995) Determination of the solution structure of apo calbindin D_{9k} by NMR spectroscopy, *J. Mol. Biol. 249*, 441–462.
12. Carlstrom, G., and Chazin, W. J. (1993) Two-dimensional 1H nuclear magnetic resonance studies of the half-saturated $(Ca^{2+})_1$ state of calbindin D_{9k}: further implications for the molecular basis of cooperative Ca^{2+} binding, *J. Mol. Biol. 231*, 415–430.
13. Julenius, K., Robblee, J., Thulin, E., B.E., F., Fairman, R., and Linse, S. (2002) Coupling of ligand binding and dimerization of helix-loop-helix peptides: spectroscopic and sedimentation analyses of calbindin D_{9k} EF-hands, *Proteins 47*, 323–333.
14. Scholtz, J. M., Barrick, D., York, E. J., Stewart, J. M., and Baldwin, R. L. (1995) Urea unfolding of peptide helices as a model for interpreting protein unfolding, *Proc. Natl. Acad. Sci. U.S.A. 92*, 185–189.
15. Edelhoch, H. (1967) Spectroscopic determination of tryptophan and tyrosine in proteins, *Biochemistry 6*, 1948–1954.
16. Stegman, T., Schoen, P., Bron, R., Wey, J., Bartoldus, I., Ortiz, A., Nieva, J. L., and Wilschut, J. (1993) Evaluation of viral membrane fusion assays. Comparison of the octadecylrhodamine dequenching assay with the pyrene excimer assay, *Biochemistry 32*, 11330–11337.
17. Ha, J.-H., and Loh, S. N. (1998) Changes in side chain packing during apomyoglobin folding characterized by pulsed thiol-disulfide exchange, *Nat. Struct. Biol. 5*, 730–737.
18. Wimberly, B., Thulin, E., and Chazin, W. J. (1995) Characterization of the N-terminal half-saturated state of calbindin D_{9k}: NMR studies of the N56A mutant, *Protein Sci. 4*, 1045–1055.
19. Skelton, N. J., Kordel, J., Akke, M., and Chazin, W. J. (1992) Nuclear magnetic resonance studies of the internal dynamics in apo, $(Cd^{2+})_1$ and $(Ca^{2+})_2$ calbindin D_{9k}, *J. Mol. Biol. 227*, 1100–1117.
20. Vogel, C., and Morea, V. (2006) Duplication, divergence and formation of novel protein topologies, *BioEssays 28*, 973–978.
21. Baird, G. S., Zacharias, D. A., and Tsien, R. Y. (1999) Circular permutation and receptor insertion within green fluorescent protein, *Proc. Natl. Acad. Sci. U.S.A. 96*, 11241–11246.
22. Perez-Jiminez, R., Garcia-Manyes, S., Ainavarapu, S. R. K., and Fernandez, J. M. (2006) Mechanical unfolding pathways of the enhanced yellow fluorescent protein revealed by single molecule force spectroscopy, *J. Biol. Chem. 281*, 40010–40014.
23. Viguera, A. R., Serrano, L., and Wilmanns, M. (1996) Different folding transition states may result in the same native structure, *Nat. Struct. Biol. 3*, 874–880.
24. Ivarsson, Y., Travaglini-Allocatelli, C., Brunori, M., and Gianni, S. (2008) Folding and misfolding in a naturally occurring circularly permuted PDZ domain, *J. Biol. Chem. 283*, 8954–8960.
25. Brinkmann, U., Di Carlo, A., Vasmatzis, G., Kurochkina, N., Beers, R., Lee, B., and Pastan, I. (1997) Stabilization of a recombinant F_v fragment by base-loop interconnection and V_H-V_L permutation, *J. Mol. Biol. 268*, 107–117.
26. Miller, E., Fischer, K. F., and Marqusee, S. (2002) Experimental evaluation of topological parameters determining protein-folding rates, *Proc. Natl. Acad. Sci. U.S.A. 99*, 10359–10363.
27. Kojima, M., and Ayabe, K. U., H. (2005) Importance of terminal residues on circularly permuted *Escherichia coli* alkaline phosphatase with high specific activity, *J. Biosci. Bioeng. 100*, 197–202.

28. Buchwalder, A., Szadkowski, H., and Kirschner, K. (1992) A fully active variant of dihydrofolate reductase with a circularly permuted sequence, *Biochemistry 31*, 1621–1630.
29. Goldenberg, D. P., and Creighton, T. E. (1983) Circular and circularly permuted forms of bovine pancreatic trypsin inhibitor, *J. Mol. Biol. 165*, 407–413.
30. Zhang, T., Bertelsen, E., Benvegnu, D., and Alber, T. (1993) Circular permutation of T4 lysozyme, *Biochemistry 32*, 12311–12318.
31. Luger, K., Hommel, U., Herold, M., Hofsteenge, J., and Kirschner, K. (1989) Correct folding of circularly permuted variants of a beta alpha barrel enzyme *in vivo*, *Science 243*, 206–210.
32. Haglund, E., Lindberg, M. O., and Oliveberg, M. (2008) Changes of protein-folding pathways by circular permutation: overlapping nuclei promote global cooperativity, *J. Biol. Chem. 283*, 27904–27915.
33. Paszkiewicz, K. H., Sternberg, M. J., and Lappe, M. (2006) Prediction of viable circular permutants using a graph theoretic approach, *Bioinformatics 22*, 1353–1358.
34. Julenius, K., Thulin, E., Linse, S., and Finn, B. E. (1998) Hydrophobic core substitutions in calbindin D_{9k}: effects on stability and structure, *Biochemistry 37*, 8915–8925.
35. Cutler, T., and Loh, S. N. (2007) Thermodynamic analysis of an antagonistic folding-unfolding equilibrium between two protein domains, *J. Mol. Biol. 371*, 308–316.
36. Pace, C. N., and Scholtz, J. M. (1997) Measuring the conformational stability of a protein, in *Protein Structure: A Practical Approach* (Creighton, T. E., Ed.) 2nd ed., pp 299—321, Oxford University Press, New York.
37. Santoro, M. M., and Bolen, D. W. (1988) Unfolding free energy changes determined by the linear extrapolation method. 1. Unfolding of phenylmethanesulfonyl alpha chymotrypsin using different denaturants, *Biochemistry 27*, 8063–8068.
38. Thulin, E. (2002) Purification of recombinant calbindin D_{9k}, *Methods Mol. Biol. 172*, 175–184.